2024 IEEE International Conference on Robotics and Automation (ICRA 2024)
May 13-17, 2024. Yokohama, Japan

Inconstant curvature kinematics of parallel continuum robot without static model

Tao Zhang[1,3], Huxin Gao[1], Hongliang Ren[1,2,3*]

***Abstract*— In the study of minimally invasive surgical robots, a mini parallel continuum robot has shown motion advantage after passing through a long and winding working channel. However, due to the interaction force between the elastic wires of the parallel robots during motion generation processes, the constant curvature assumption has shown modeling errors. This causes the current geometric kinematic model to become unreliable. Therefore, there is a need for a more accurate kinematic model in the absence of a complicated static model. This paper aims to solve this issue. The simulation in ANSYS is carried out, and the shape of one of the driving wires, when bending, is fitted by a two-segment polynomial curve. Then, the position of the distal wrist tip can be calculated based on the curve shape. To verify the accuracy of the proposed model, bending simulation and experiment are carried out. The accuracy of the proposed model is compared with that of the kinematic model based on constant curvature assumption. The result shows that the proposed model can get more accurate results, especially when the driving wire displacement increases. For a 10 mm parallel robot, when the displacements of the two pairs of wires are both 3.0 mm, the errors of the two models are 0.42 mm and 5.79 mm (4.2% and 57.9%), respectively.**

I. Introduction

Flexible manipulators have become essential parts of robot-assisted gastrointestinal endoscopic surgery (GES) [1], such as flexible parallel robots [2] [3], single-backbone continuum robots [4] [5], and redundant robots [6]. The flexibility of the manipulators can adjust the long and winding working channel of GES well but also increase the difficulty of kinematic modeling. For a parallel continuum robot, the bending motion relies on the deformation of the elastic wires, which is nonlinear. Therefore, it is hard to get an accurate kinematic model using the current analytical model, such as the constant curvature assumption [7]. To solve this problem, researchers are proposing more accurate kinematic models.

The kinematic model of a flexible continuum manipulator has been built by using nonlinear elastic rod model assumptions, such as the Cosserat rod theory [8], the Kirchhoff-Love beam theory [9] and the Euler-Bernoulli beam theory [10], the shape of the manipulator can be calculated when the external force and torque are given. In addition, the Cosserat rod theory was also adopted in the kinematic model of a six-rod parallel flexible robot [11]. The mechanical and geometric constraints were treated as boundary conditions, and the shape of each elastic rod was calculated using the Cosserat rod theory. However, when adopting nonlinear elastic rod theories, the kinematic model always needs a complicated numerical computation procedure [12].

To improve computational efficiency, we can work from two aspects: the first is to optimize the solving method of the equations with boundary conditions [13], and the second is to adopt a static model-free approach to model the robots. The curve fitting method has been proposed for the continuum robots with a single backbone. For example, the Euler curve was introduced into the kinematic modeling of the continuum robot [14], and the accuracy was validated in a pneumatic continuum robot. Then, further research was also introduced in single backbone continuum robot [15] and catheter with large deformation [16]. In reference [15], aiming at a continuum robot with an elastic backbone and several driving tendons, the relationship between the robot shape and the external forces was obtained when the driving length of the tendons. In addition, the torsion angle distribution along each segment in a continuum robot was also assumed to follow the arithmetic series distribution [17].

Other curves were also used in the kinematic model, such as the polynomial curve [18] and Pythagorean Hodograph curve [19]. In these papers, the shape of the elastic elements is assumed to be a specific curve with several unknown parameters, and the kinematic model can be obtained by identifying these parameters.

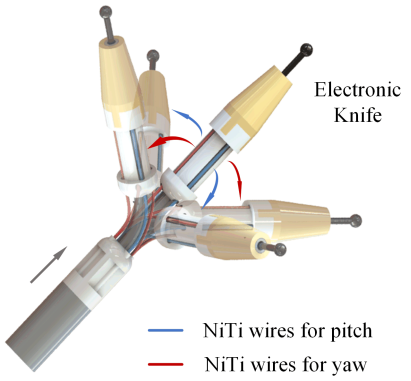

Fig. 1. Our previous flexible wrist applied in ESD [20].

In the previous work, a parallel continuum robot has been proposed as a flexible wrist to perform the endoscopic submucosal dissection (ESD) (Fig. 1) [20] [21]. Four NiTi wires work as both driving wires and flexible backbones.

This work was supported in part by Hong Kong Research Grants Council (RGC) Collaborative Research Fund (CRF C4026-21GF), and General Research Fund (GRF 14216022, GRF 14203323); Guangdong Basic and Applied Basic Research Foundation (GBABF) #2021B1515120035.

[1]Dept. of Electronic Engineering, The Chinese University of Hong Kong (CUHK), Hong Kong SAR, China; [2]Shun Hing Institute of Advanced Engineering, CUHK, Hong Kong SAR, China; [3]Shenzhen Research Institute, The Chinese University of Hong Kong, Shenzhen 518063 China
*Corresponding author: Hongliang Ren (hlren@ieee.org)

The current kinematic model of the robot is built under the constant curvature assumption. However, with the bending angle growing, the constant curvature assumption's error also increases. To solve this issue, we proposed an inconstant curvature kinematic model of the flexible parallel robot without a static model, the key contribution of this work is shown as follows.

1). A two-segment curve with varied curvature is used to modeling the deformation of the flexible parallel wrist, which shows higher accuracy compared with the curve with constant curvature.

2). Due to the use of the geometric method, the proposed model needs less numerical calculation, which is preferred by real-time control.

In the rest of this paper, based on a simulation-to-reality approach [22], the shapes of the NiTi wires with different driving displacements exerted are obtained through ANSYS simulation. A two-segment symmetrical polynomial curve is used to fit the shape of a chosen wire, and the posture of the symmetry axis is obtained by the proportional curvature assumption. Using simulation results, we verify the accuracy of this curve to fit the shape of the chosen wire compared with a constant curvature curve (an arc). Finally, a verification experiment is also conducted, showing the proposed model's higher accuracy.

II. Modeling and System Identification

A. Analysis and simplification of the parallel robot deformation

As shown in Fig.2, the driving displacements of the four NiTi wires are 5, 5, -5, and -5 mm (The driving displacement is the length variation of a NiTi wire. The positive value means that the wire is pulled and the negative value means the wire is pushed). The three-dimensional shapes of the four NiTi wires are obtained by using the ANSYS workbench. For wire 1, the prediction shape under the constant curvature assumption differs from the simulation result because of the interaction force between the four wires.

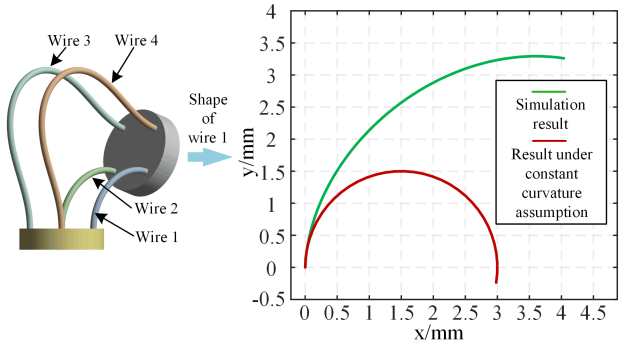

Fig. 2. Comparison of the simulation result and the constant curvature assumption.

In Fig.3, under the isolation method, the constraints of the driving wires on proximal and distal sides are both the limitations of three directions displacement and three directions rotation. Then, we can assume that: $|F_{21}| = \left|F_{21}^{'}\right|, |F_{22}| = \left|F_{22}^{'}\right|, |M_2| = \left|M_2^{'}\right|, |F_{31}| = \left|F_{31}^{'}\right|, |F_{32}| = \left|F_{32}^{'}\right|, |M_3| = \left|M_3^{'}\right|$, and the direction of the corresponding pairs of forces or torques are symmetric about the midpoint of the wire. For a micro-element, the stress includes axial stress F_{m1} and F_{m2}, circumferential stress F_{m3} and F_{m4}, and the moment M_{m1} and M_{m2}. In each cross-section, the internal force and moment can be obtained as follows:

$$\begin{cases} F_t = F_{m2} + F_{m1} = F_{21}^{'} + F_{22}^{'} \\ M_t = M_{m1} = M_2^{'} + F\left(P_{micro} - P_{distal}\right) \end{cases}, \tag{1}$$

where P_{micro} and P_{distal} are the positions of the cross-section center and the distal tip center separately. The magnitude of M_t is determined by the relative position between P_{micro} and P_{distal} when F_t is constant. The bending angle of each microelement can be obtained by: $M_t = diag[EI_x, EI_y, EI_z]u$, where u is the strain of the microelement.

The former equations indicate that the curvature varies along the wire due to F_{m2} and F_{m1}. When there is no external force applied on the distal tip of the robot, the distribution of M_t and curvature are both symmetrical, and the curvature at the midpoint of a wire is the largest point.

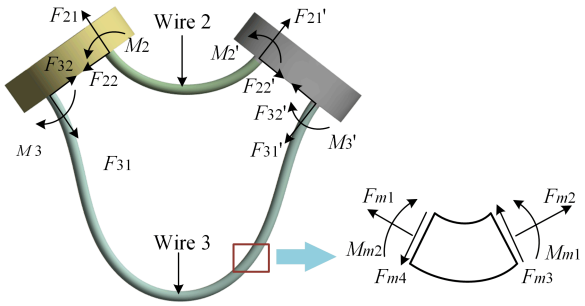

Fig. 3. Static model and micro-element analysis of the NiTi wires.

B. Choosing and shape fitting of the NiTi wire

As shown in Fig.1, the driving wires of the robot could be divided into two groups: NiTi wires for pitch and yaw. Each group has two antagonistic drive wires, and the absolute driving displacements of the two wires are the same. Then, with the bending angle growing, the pushing wires will experience a complex bending behavior, shown in Fig.3. However, the pulling wires show simpler shapes. If we can get the tip position and corresponding orientation of a pulling wire, we can calculate the tip position and the tip orientation of the robot by using the geometric method.

Choose the shorter pulling wire, and we can get the center position of the distal disk as follows.

As shown in Fig. 4, the distal tip position of the wire is T, and the orientation of the distal wire tip is K, which is the same as that of the distal disk. Then, we can get that:

$$P_{ot} = T + r\left[cos\theta cos\Phi \quad cos\theta sin\Phi \quad sin\theta\right], \tag{2}$$

where P_{ot} is the position of the distal disk center, r is the distance between the wire hole and the disk center, θ is the bending angle and Φ is the deflection angle.

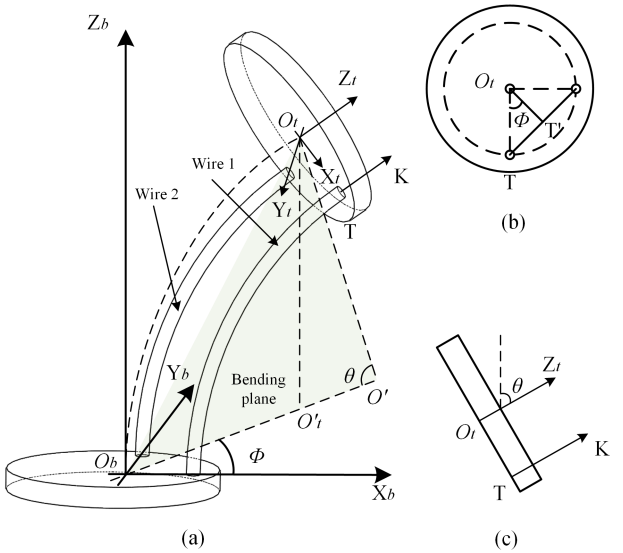

Fig. 4. Coordinate system of the parallel robot: (a) Coordinate system fixed on the robot. (b-c) Partial views of the distal tip.

From the references, the Euler curve has shown the potential to describe the shape of an elastic wire with external force applied. However, an Euler curve does not have an analytical form for the position of any curve segment, and the formula is shown as follows:

$$\begin{cases} x = \int_0^x sint^2 dt \\ y = \int_0^x cost^2 dt \end{cases} \tag{3}$$

where x and y are the coordinate values of the tip of an Euler curve segment whose curve length is t. The above function contains Fresnel calculus, which cannot be described by elementary function. To solve this problem, we proposed a compliant method. The property of the Euler curve was used to define the chosen NiTi wire's bending angle and a polynomial curve(quadratic curve) was used to describe the tip position of the chosen NiTi wire. When given the curve length, a quadratic function can get the corresponding coordinate values. Assuming the function is $y = kx^2$, the curve length of the curve can be obtained as (4).

$$\begin{aligned} L &= \int_0^x \sqrt{1+4k^2x^2}dx \\ &= \frac{x}{2}\sqrt{1+4k^2x^2} + \frac{1}{4k}ln\left(2kx + \sqrt{1+4k^2x^2}\right) \end{aligned} \tag{4}$$

When given (4), the value of x can be solved simply by using a numerical method.

The shape of the chosen wire is divided into two segments, and under the former assumption, the parallel robot is a symmetrical structure when the driving values remain constant. Therefore, the spatial shape of the NiTi wire can be assumed to be symmetrical, and the junction of the two segments is the midpoint of each wire.

As shown in Fig.5, M and E are the middle point and the distal tip of a wire separately, the solving process is shown as follows.

To get the bending angle of the middle point of the wire, referring to the property of the Euler curve, we can get:

$$\frac{\theta}{2} = \int_0^{0.5l_{total}} vsds = \frac{vl_{total}^2}{8}. \tag{5}$$

Then, the position of M can be calculated as follows:

$$P_M = \begin{bmatrix} L_{OM'}cos\Phi & L_{OM'}\Phi sin & \sqrt{\frac{L_{OM'}}{k}} \end{bmatrix}, \tag{6}$$

where P_M and P_E are the position of M and E concerning coordinate XYZ. Φ is the deflection angle of the wire. For a pulling wire, we can get:

$$\Phi = atan\frac{dl_2}{dl_1}, \tag{7}$$

where dl_1 and dl_2 are the driving values of pulling wire 1 and wire 2. By getting the position and bending angle of M, the position and orientation of the distal tip are shown as follows:

$$\begin{cases} k_0 = -tan\frac{\theta}{2} \\ b = \sqrt{\frac{L_{OM'}}{k_0}} - k_0 L_{OM'} \\ P_E = \begin{bmatrix} \frac{-2bk_0}{k_0+1}cos\Phi & \frac{-2bk_0}{k_0+1}sin\Phi & \frac{-2k_0^2}{k_0+1} + 2b \end{bmatrix} \end{cases} \tag{8}$$

C. Forward kinematics

At first, assume that the driving displacements of the four wires are dl_1, dl_2, dl_3, and dl_4. Then, as the parallel robot is driven by two motors and two two-way lead screws, we can obtain that: $dl_1 = -dl_3$, $dl_2 = -dl_4$. The deflection angle of the wrist can be calculated easily by (7).

To get the bending shape of the NiTi wires, as shown in the former content, the coefficients v and k need to be obtained first. To get the coefficients, a series of simulations are carried out in ANSYS. Three typical driving displacement ratios of wire 1 and wire 2 are adopted, which are 1:0, $\sqrt{3}$:1, and 1:1. Then, the driving displacement of wire 1 varies from 0 to 3.0 mm (the max bending angle is around 90°). By fitting the shapes of the driving wires, we can get the k and v in each pair of driving displacements.

For the coefficient v, under the three typical angles, the value of v corresponding to the driving value of wire 1 can be shown in Table. I.

TABLE I
COEFFICIENT v OF THE WRIST

dl_2 /mm	dl_1/mm					
	0.5	1.0	1.5	2.0	2.5	3.0
$l_1 * 0$	0.0146	0.0318	0.0498	0.0721	0.0965	0.1260
$l_1/\sqrt{3}$	0.0165	0.0348	0.0540	0.0733	0.0950	0.1161
$l_1 * 1$	0.0200	0.0419	0.0632	0.0857	0.1082	0.1341

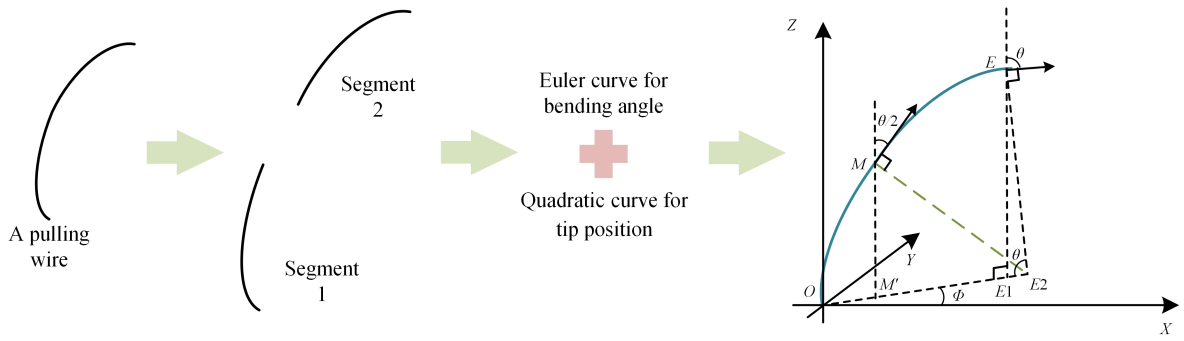

Fig. 5. The curve fitting progress: The shape of the chosen wire is symmetrical, and the shape can be divided into segment 1 and segment 2, which have the same shape and different positions and posture, The distal tip of segment 1 is the proximal tip of segment 2. The inclination angle of the axis of symmetry between the two segments is obtained by curve fitting results, and the shape of each segment is a quadratic curve.

TABLE II

COEFFICIENT k OF THE WRIST

dl_2 /mm	dl_1/mm					
	0.5	1.0	1.5	2.0	2.5	3.0
$l_1 * 0$	7.200	4.805	3.805	3.120	2.623	2.400
$l_1/\sqrt{3}$	6.926	4.344	3.483	3.010	2.725	2.558
$l_1 * 1$	5.880	4.005	3.272	2.842	2.591	2.395

The relationship between the dl_1 and the v could be easily expressed by using a polynomial model. For the first scenario, the relationship is:

$$v = 0.006209dl_1^2 + 0.02245dl_1 + 0.002291. \tag{9}$$

For the coefficient k, under the three typical driving displacement ratios, the value of k corresponding to the driving displacement of wire 1 can be shown in Table. II.

The relationship between the dl_1 and the k could also be easily expressed by using a polynomial model. For the first scenario, the relationship is:

$$k = 0.3887dl_1^4 - 3.1641dl_1^3 + 9.73dl_1^2 - 14.54dl_1 + 12.41. \tag{10}$$

The fitting progress of k and v when the driving displacement ratio varies among the three scenarios can be shown in Fig. 6 and Table. II.

The fitting results of the chosen NiTi wire shape are shown in Fig. 7. Fig. 2 and Fig. 7 show that the proposed model can fit the driving shape wire better. When the driving displacement increases, the position error of the proposed curve remains negligible, while the position error of a constant curvature curve experiences a sharp increase.

Then, we can get the orientation and position of the midpoint of the pulling wires. The bending angle is:

$$\theta_m = \frac{v\left(l_0 - dl_1\right)^2}{8}. \tag{11}$$

The position is:

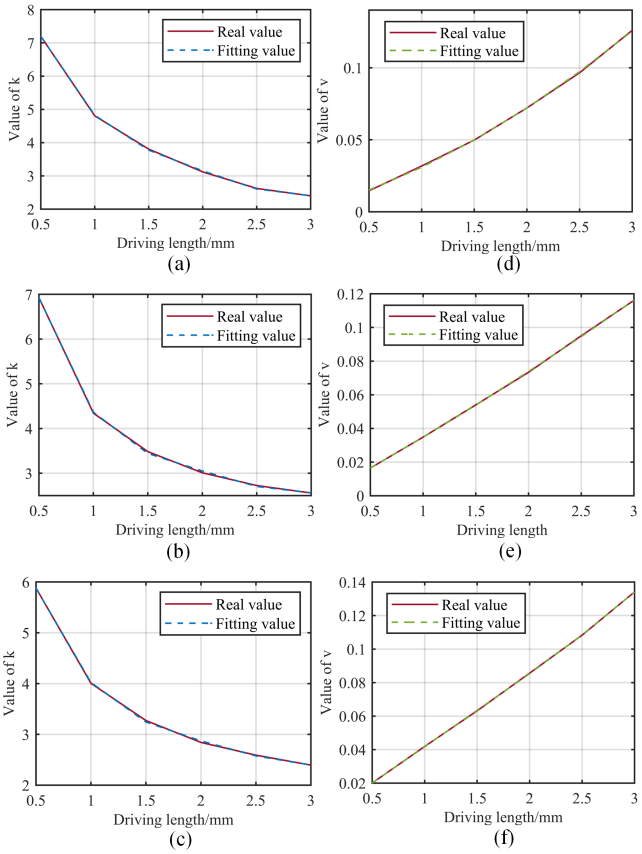

Fig. 6. The fitting results of k and v: (a-c) The fitting result of k in three scenarios: $dl_2/dl_1 = 0$, $dl_2/dl_1 = \sqrt{3}/3$, $dl_2/dl_1 = 1$, (d-f) The fitting result of v in three scenarios.

$$P = \begin{bmatrix} x_0 cos\Phi & x_0 sin\Phi & k\sqrt{x_0}. \end{bmatrix}. \tag{12}$$

Under the symmetry assumption, the orientation and position of the distal tip of the pulling wires can be obtained by (8). The transformation matrix between the base coordinate system $X_bO_bY_b$ and the distal tip coordinate system $X_tO_tY_t$ can be shown as follows:

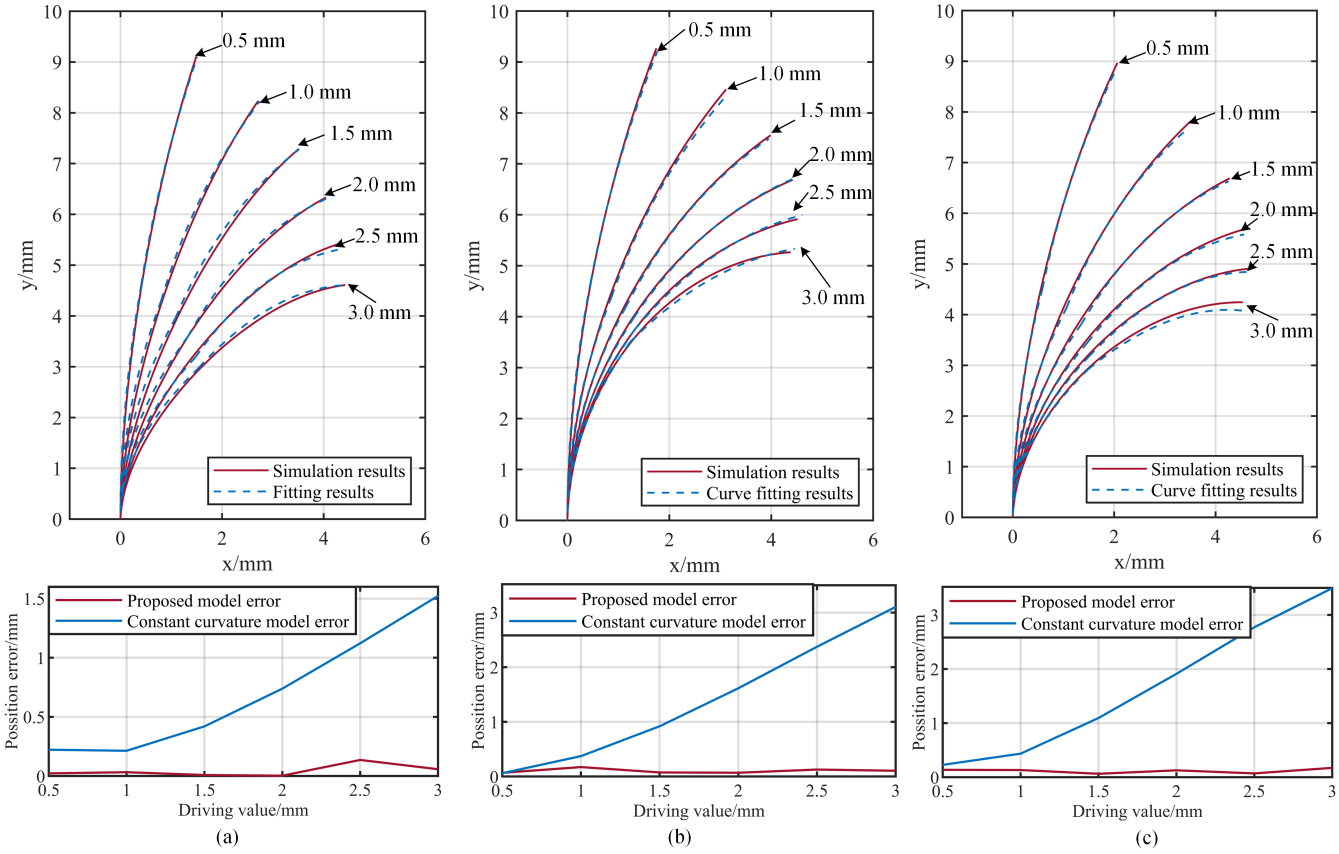

Fig. 7. Comparison of the simulation results and the fitting results, and the tip position error of each scenario: (a) The driving displacement of wire 1 varies from 0.5 to 3.0 mm, and the driving displacement of wire 2 is 0 mm. (b) The driving displacement of wire 1 varies from 0.5 to 3.0 mm, and the driving displacement of wire 2 is $dl_2 = dl_1/\sqrt{3}$.(c) The driving displacement of wire 1 varies from 0.5 to 3.0 mm, and the driving displacement of wire 2 is $dl_2 = dl_1$.

TABLE III

POSITION ERROR OF THE PROPOSED MODEL AND THE CONSTANT CURVATURE MODEL

dl_2	dl_1/mm					
$/mm$	0.5	1.0	1.5	2.0	2.5	3.0
$l_1 * 0$	0.563/0.335	0.654/0.785	0.961/1.074	1.072/1.582	1.095/2.335	1.048/3.018
$l_1/\sqrt{3}$	0.108/1.073	0.501/1.377	0.801/1.934	0.945/2.705	1.031/3.575	1.292/4.525
$l_1 * 1$	0.421/1.288	0.464/1.624	0.495/2.476	0.305/3.602	0.302/4.797	0.416/5.791

Assume that T_{xr}, T_t, $T_{z\Phi}$, $T_{y\theta}$, $T_{z(-\Phi)}$, and $T_{x(-r)}$ are the transformation matrixes from the base coordinate to the target coordinate. T_{xr} refers to the translation from the center of the proximal disk to the base of the wire, T_r refers to the translation from the proximal tip of the wire to the distal tip of the wire, $T_{z\Phi}$ refers to the rotation Φ about the Z-axis, $T_{z\theta}$ refers to the rotation θ about X-axis, $T_{z(-\Phi)}$ refers to the rotation -Φ about Z-axis, $T_{x(-r)}$ refers to the translation from the distal tip of the wire to the center of the distal disk.

$$T_{xr} = \begin{bmatrix} & r \\ E & 0 \\ & 0 \\ 0 & 0 \end{bmatrix}, T_t = \begin{bmatrix} & -2b/\left(k_0 + 1/k_0\right) c\Phi \\ E & -2b/\left(k_0 + 1/k_0\right) s\Phi \\ & -2k_0 b/k_0 + 1/k_0 + 2b \\ 0 & 1 \end{bmatrix},$$

$$T_{z\Phi} = \begin{bmatrix} c\Phi & -s\Phi & 0 & 0 \\ s\Phi & c\Phi & 0 & 0 \\ 0 & 0 & 1 & 0 \\ 0 & 0 & 0 & 1 \end{bmatrix}, T_{x\theta} = \begin{bmatrix} c\theta & 0 & s\theta & 0 \\ 0 & 1 & 0 & 0 \\ -s\theta & 0 & c\theta & 0 \\ 0 & 0 & 0 & 1 \end{bmatrix},$$

$$T_{z-\Phi} = \begin{bmatrix} c\Phi & s\Phi & 0 & 0 \\ -s\Phi & c\Phi & 0 & 0 \\ 0 & 0 & 1 & 0 \\ 0 & 0 & 0 & 1 \end{bmatrix}, T_{x-r} = \begin{bmatrix} & -r \\ E & 0 \\ & 0 \\ 0 & 1 \end{bmatrix}.$$

The whole transformation matrix T_{bt} can be calculated as (13).

$$T_{be} = T_{xr} T_t T_{z\Phi} T_{v\theta} T_{z(-\Phi)} T_{x(-r)}. \tag{13}$$

D. Inverse kinematics

For a flexible parallel continuum robot, the orientation and position of the distal tip are coupled without external force or

torque. As a result, the driving displacement can be obtained by using the orientation of the distal tip. Set the desired orientation is $[sin\theta cos\Phi, sin\theta sin\Phi, cos\theta]$. Then, we can get (14).

$$\frac{vdl_1\left(l_0 - dl_1\right)^2}{4} = \theta \tag{14}$$

Assume that $v = adl^2 + bdl + c$, the (14) can be transformed into (15):

$$\begin{aligned} 0 = {} & adl_1^4 + \left(b - 2al_0\right) dl_1^3 + \\ & \left(al_0^2 - 2bl_0 + c\right) dl_1^2 + \left(bl_0^2 - 2cl_0\right) dl_1 + cl_0^2 - 4\theta \end{aligned} \tag{15}$$

By solving the above equation, the value of dl_1 can be obtained. Then, dl_2 can be calculated by (7)

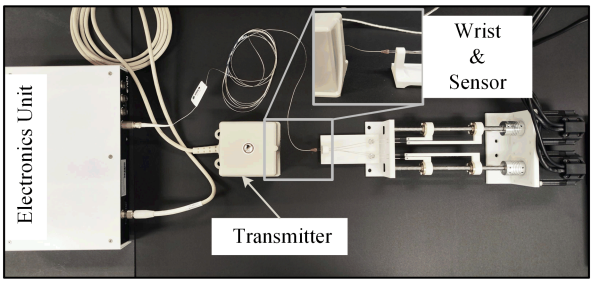

Fig. 8. The experimental platform

III. Experiment Verification

To verify the accuracy of the curve-fitting kinematic model, the position and posture of the distal tip of a parallel robot are measured and compared with the result based on the proposed kinematic model. The experimental platform is shown as Fig. 8. In the experiment, the robot length is 10 mm, the distance of two opposite driving wires is 3.0 mm, and the diameter of the driving wires is 0.3 mm. The four NiTi wires are driven by two two-way lead screws. The 3D position and posture of the distal tip are measured by a 3D Guidance trakSTAR (Ascension Technology Corporation (ATC)). The position error of the proposed model is shown as Fig. 9 and Table. III.

The experiment results show that the position error of the proposed model is much less than that based on the constant curvature assumption. When the two pairs of NiTi wires are fed at different driving displacement ratios, the accuracy of the kinematics model under constant curvature assumption is lower than that of the proposed kinematics model. When the driving displacement of wire 1 is 3.0 mm, the position errors of the two models are 1.048 mm/3.018 mm, 1.292 mm/4.525 mm, and 0.416 mm/5.791 mm under different driving displacement ratios.

In another aspect, when the bending motion is symmetrical(the driving ratio is 1), we can get that the error is less than that when the ratio is 0 or $\sqrt{3}$. This phenomenon shows that for a flexible parallel robot, the unsymmetrical motion might cause a larger motion error. The reasons might come from the different contact forces between the driving wires and their working channels.

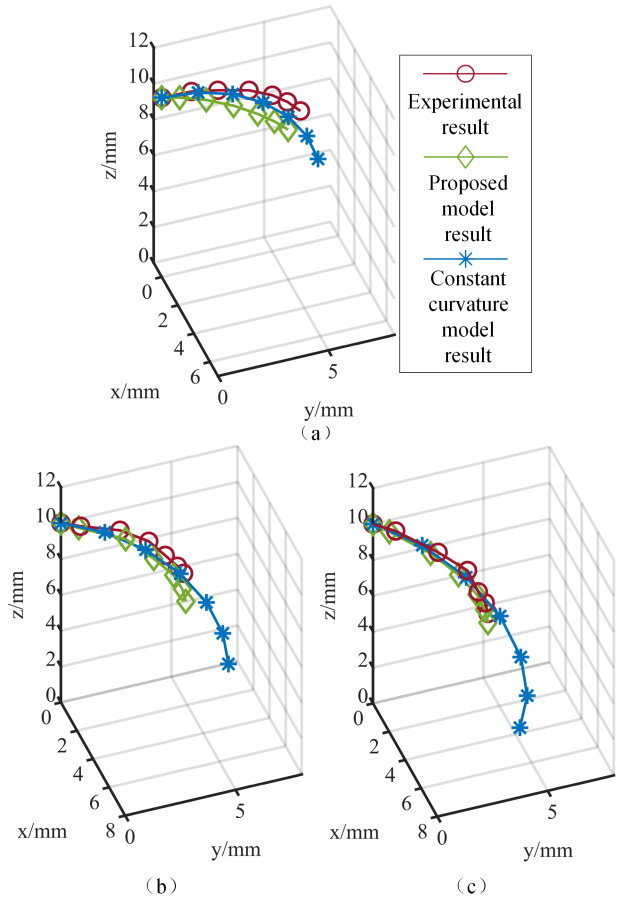

Fig. 9. The experimental results: (a) Position error of a 2-D motion. (b) Position error of a 3-D motion when the driving ratio is $\sqrt{3}$. (c) Position error of a 3-D motion when the driving ratio is 1. In the three figures, each point refers to a data collection point.

IV. Conclusion

This paper proposed an inconstant curvature kinematic model for a parallel flexible robot without building the static model. The pulling NiTi wire with less driving displacement is chosen as the research object. Its bending shape is fitting using a two-segment polynomial curve and an Euler angle. The position of the distal tip can be calculated based on it. Compared with the kinematic model based on constant curvature assumption, the position accuracy of the proposed model is higher, and due to the absence of the static model in this approach, the complicated computational process will be avoided too.

The research also shows that the model will have higher accuracy when experiencing a symmetrical motion, which means that the next step of this research is to consider the interaction between different driving wires. In addition, in this research, the motion is limited to several directions, therefore, our future work will study the bending shape in a random direction.

References

[1] P. E. Dupont, N. Simaan, H. Choset, and C. Rucker, "Continuum robots for medical interventions," *Proceedings of the IEEE*, vol. 110,

no. 7, pp. 847–870, 2022.
[2] Y. Yang, J. Li, K. Kong, and S. Wang, "Design of a dexterous robotic surgical instrument with a novel bending mechanism," *The International Journal of Medical Robotics and Computer Assisted Surgery*, vol. 18, no. 1, p. e2334, 2022.
[3] X. Yang, H. Gao, S. Fu, R. Ji, C. Hou, H. Liu, N. Luan, H. Ren, L. Sun, J. Yang, *et al.*, "Novel miniature transendoscopic telerobotic system for endoscopic submucosal dissection (with videos)," *Gastrointestinal Endoscopy*, vol. 99, no. 2, pp. 155–165, 2024.
[4] H. Gao, Z. Zhang, C. Li, X. Xiao, L. Qiu, X. Yang, R. Hao, X. Zuo, Y. Li, and H. Ren, "Gesrsim: Gastrointestinal endoscopic surgical robot simulator," in *2022 IEEE/RSJ International Conference on Intelligent Robots and Systems (IROS)*, pp. 9542–9549, IEEE, 2022.
[5] C. Li, X. Gu, X. Xiao, C. M. Lim, X. Zuo, Y. Li, X. Duan, and H. Ren, "Deployable parallelogram mechanism and constrained bendable segment for flexible robot toward transoral procedures," *IEEE Transactions on Medical Robotics and Bionics*, 2023.
[6] H. Gao, R. Hao, X. Yang, C. Li, Z. Zhang, X. Zuo, Y. Li, and H. Ren, "Modeling and compensation of stiffness-dependent hysteresis for stiffness-tunable tendon-sheath mechanism in flexible endoscopic robots," *IEEE Transactions on Industrial Electronics*, 2023.
[7] Z. Wang, S. Bao, B. Zi, Z. Jia, and X. Yu, "Development of a novel 4-dof flexible endoscopic robot using cable-driven multisegment continuum mechanisms," *Journal of Mechanisms and Robotics*, vol. 16, no. 3, p. 031011, 2024.
[8] G. Wu and G. Shi, "Design, modeling, and workspace analysis of an extensible rod-driven parallel continuum robot," *Mechanism and Machine Theory*, vol. 172, p. 104798, 2022.
[9] H. Yuan, L. Zhou, and W. Xu, "A comprehensive static model of cable-driven multi-section continuum robots considering friction effect," *Mechanism and Machine Theory*, vol. 135, pp. 130–149, 2019.
[10] J. Liu, S. Shang, G. Zhang, S. Xue, H. Cheng, P. Qi, and F. Du, "Curvature correction of a notched continuum robot based on a static model considering large deformation and friction effect," *Machines*, vol. 10, no. 9, p. 778, 2022.
[11] C. E. Bryson and D. C. Rucker, "Toward parallel continuum manipulators," in *2014 IEEE International Conference on Robotics and Automation (ICRA)*, pp. 778–785, IEEE, 2014.
[12] G. Wu and G. Shi, "Experimental statics calibration of a multi-constraint parallel continuum robot," *Mechanism and Machine Theory*, vol. 136, pp. 72–85, 2019.
[13] J. Till, C. E. Bryson, S. Chung, A. Orekhov, and D. C. Rucker, "Efficient computation of multiple coupled cosserat rod models for real-time simulation and control of parallel continuum manipulators," in *2015 IEEE international conference on robotics and automation (ICRA)*, pp. 5067–5074, IEEE, 2015.
[14] P. S. Gonthina, A. D. Kapadia, I. S. Godage, and I. D. Walker, "Modeling variable curvature parallel continuum robots using euler curves," in *2019 International Conference on Robotics and Automation (ICRA)*, pp. 1679–1685, IEEE, 2019.
[15] P. Rao, Q. Peyron, and J. Burgner-Kahrs, "Using euler curves to model continuum robots," in *2021 IEEE International Conference on Robotics and Automation (ICRA)*, pp. 1402–1408, IEEE, 2021.
[16] M. Srivastava, J. Ammons, A. B. Peerzada, V. N. Krovi, P. Rangaraju, and I. D. Walker, "3d printing of concrete with a continuum robot hose using variable curvature kinematics," in *2022 International Conference on Robotics and Automation (ICRA)*, pp. 3216–3222, IEEE, 2022.
[17] P. Rao, Q. Peyron, and J. Burgner-Kahrs, "Shape representation and modeling of tendon-driven continuum robots using euler arc splines," *IEEE Robotics and Automation Letters*, vol. 7, no. 3, pp. 8114–8121, 2022.
[18] F. Stella, N. Obayashi, C. Della Santina, and J. Hughes, "An experimental validation of the polynomial curvature model: identification and optimal control of a soft underwater tentacle," *IEEE Robotics and Automation Letters*, vol. 7, no. 4, pp. 11410–11417, 2022.
[19] I. Singh, Y. Amara, A. Melingui, P. Mani Pathak, and R. Merzouki, "Modeling of continuum manipulators using pythagorean hodograph curves," *Soft robotics*, vol. 5, no. 4, pp. 425–442, 2018.
[20] H. Gao, X. Xiao, X. Yang, T. Zhang, X. Zuo, Y. Li, and H. Ren, "A miniature 3-dof flexible parallel robotic wrist using niti wires for gastrointestinal endoscopic surgery," *arXiv preprint arXiv:2207.04735*, 2022.
[21] H. Gao, X. Yang, X. Xiao, X. Zhu, T. Zhang, C. Hou, H. Liu, M. Q.-H. Meng, L. Sun, X. Zuo, *et al.*, "Transendoscopic flexible parallel continuum robotic mechanism for bimanual endoscopic submucosal dissection," *The International Journal of Robotics Research*, vol. 43, no. 3, pp. 281–304, 2024.
[22] J. Lai, T.-A. Ren, W. Yue, S. Su, J. Y. Chan, and H. Ren, "Sim-to-real transfer of soft robotic navigation strategies that learns from the virtual eye-in-hand vision," *IEEE Transactions on Industrial Informatics*, 2023.